Reconstructing NMR images under magnetic fields with large inhomogeneities

1982 J. Phys. E: Sci. Instrum. 15 1093

(http://iopscience.iop.org/0022-3735/15/10/031)

J. Phys. E: Sci. Instrum., Vol. 15, 1982. Printed in Great Britain

Reconstructing NMR images under magnetic fields with large inhomogeneities

Ching-Ming Lai
Analogic Corporation, Audubon Road, Wakefield, Mass 01880, USA

Received 10 March 1982

Abstract. A novel technique is presented for reconstructing accurate NMR images from projections under inhomogeneous main magnetic field. The mathematical basis and the point-spread functions of such a curvilinear reconstruction for two- and three-dimensional imagings are fully described. The proper use and the effectiveness of this technique are demonstrated by computer simulations. The promising results presented here could strongly influence practices in the design, manufacture and use of the main magnet for NMR imaging by the projections method.

1. Introduction

One way of obtaining a nuclear magnetic resonance (NMR) image is reconstructing the image from projections. When a uniform magnetic field is superimposed by a linear field gradient, the NMR spectrum represents a rectilinear projection of the object, namely the plane integral of the nuclear spins in resonance, perpendicular to the gradient direction. A three-dimensional (3D) image of the object within the active volume of the radiofrequency coil can be reconstructed from a set of such projections evenly oriented in the 3D space (Lai and Lauterbur 1980, Lai 1981). If the object is selectively excited, or selectively detected, over a thin slice, the projection becomes line integrals of the slice. The image of the slice can be reconstructed in the same way as in 2D parallel-beam x-ray tomography.

In practice, the magnetic field is not perfectly homogeneous. The projection is, in general, curved integrals. Furthermore, the curvatures and the widths of the integral paths vary from one projection angle to the other. The reconstructed image would be blurred if these integrals were treated as rectilinear. A similar imaging problem exists in acoustics, geophysics and optics where the integral paths are curved and depend on the speed of sound, or on the index of refractions, of the objects themselves. The problem in these areas remains largely unsolved.

The field uniformity is mainly determined by the design and manufacture of the magnet as well as by the interaction between the field and the ferromagnetic materials surrounding the magnet. For medical imaging at field strength of about 0.2 T (tesla), the magnetic susceptibility of a human body does not appear to cause significant perturbation of the field. In the past, the effort has been to perfect the magnet and to minimise external disturbances. Beyond that, large field gradients are used to overcome residual inhomogeneities, so that accurate images can be obtained by rectilinear reconstruction algorithms. However, technical difficulties as well as construction costs rise sharply in perfecting the magnet system. It is also desirable to reduce the field gradient strength, since large field gradients widen the NMR signal bandwidth; this wider bandwidth not only decreases the signal-to-noise ratio but also introduces more phase and amplitude errors.

Once the magnet is installed and adjusted, the magnetic field can be measured over the regions of interest. So long as the surrounding materials are undisturbed and the magnet is rigidly constructed, the same field map can be used for a long period of time. Based on the field distribution, the integral paths can be calculated for any projection angle. A set of such curved projections might provide adequate information for calculating the image by an iterative reconstruction algorithm. However, the iterative algorithm requires extensive data processing, and its reconstruction speed is at least an order of magnitude slower than that for the filtered back-projection algorithm. Furthermore, its accuracy depends on the number of iterations and the nature of the image to be reconstructed.

Although it is known that imaging information can be recovered for the sensitive-point imaging method (Hinshaw 1976) and the selective-excitation imaging method (Hutchison *et al* 1978) under magnetic fields with large non-uniformities, the information obtained by the projections method has been believed to be irretrievably lost once the non-uniformity exceeds a narrow limit (Hutchison *et al* 1978). Here, for the first time and contrary to that belief, a curvilinear filtered back-projection technique is proposed and demonstrated for reconstructing NMR images under non-uniform fields. In this paper the gradient coils are assumed to generate linear field gradients. The point-spread functions of this reconstruction technique are explicitly derived and discussed for 2D and 3D imagings. Computer simulations are then used to perform 2D imaging experiments. Throughout this paper the images are referred to the spatial distribution of nuclear densities, the parameters to be measured are obviously irrelevant to the reconstruction technique; this technique is equally applicable to imagings on NMR relaxation times.

2. Mathematical analysis

The projection paths in NMR imaging depend on the magnetic field strength in local regions. In the first step, the nature of the projection as well as its dependence on the local field and the local nuclear density will be explored. Once a strict relation between the magnetic field and the nuclear density is established, the point-spread function (PSF) of reconstructing NMR images in a uniform magnetic field will be derived and examined. Based on the behaviour of the PSF, we then look for a curvilinear reconstruction algorithm which maintains a narrow PSF under inhomogeneous magnetic field. The analysis will begin with the 3D volume reconstruction, followed by 2D slice imaging.

2.1. *The projection of an NMR image*

Let us separate the main magnetic field into

$$B(\boldsymbol{r}) = B_0 + b_0(\boldsymbol{r}) \tag{1}$$

where B_0 is the dominating space-independent field and $b_0(\boldsymbol{r})$ is the space-dependent inhomogeneity. For imaging, linear field gradients are superimposed upon the main field $B(\boldsymbol{r})$. In directing the gradient toward the orientation (θ, φ) in spherical coordinates, the currents in x, y and z gradient coils are properly controlled to produce a resultant field (Lai and Lauterbur 1980)

$$\begin{aligned} b_g(\boldsymbol{r}, \boldsymbol{u}) &= G(x \sin\theta \cos\varphi + y \sin\theta \sin\varphi + z \cos\theta) \\ &= G\boldsymbol{r} \cdot \boldsymbol{u} \end{aligned} \tag{2}$$

where $\boldsymbol{u}$ is a unit vector pointed to (θ, φ) and G is the strength of the gradient. The total space-dependent field has

$$b(\boldsymbol{r}, \boldsymbol{u}) = b_0(\boldsymbol{r}) + b_g(\boldsymbol{r}, \boldsymbol{u}). \tag{3}$$

The magnitude of $b(\boldsymbol{r}, \boldsymbol{u})$ is so much smaller than B_0 that we are only concerned with the component of $b(\boldsymbol{r}, \boldsymbol{u})$ in the direction of B_0 (Lai and Lauterbur 1980).

The NMR signal represents the evolution of the nuclear spins, each of which precesses at an angular frequency proportional to its local field strength, observed grossly following a

radiofrequency pulse excitation. In the presence of a field gradient, we may write the NMR signal detected at the frequency $\omega_0 = \gamma B_0$ as

$$V_{\theta\varphi}(t) = \exp(-\mathrm{i}\omega_0 t) \int F(\boldsymbol{r}) \exp[\mathrm{i}\gamma(B + b_g)t]\, \mathrm{d}\boldsymbol{r}$$

where γ is the gyromagnetic ratio and $F(\boldsymbol{r})$ is the density of the nuclear spins. The time domain signal $V_{\theta\varphi}(t)$ is real when it is single-phase detected, or complex if dual-phase detection is employed. Using equations (1) and (3), the equation above becomes

$$V_{\theta\varphi}(t) = \int F(\boldsymbol{r}) \exp[\mathrm{i}\gamma b(\boldsymbol{r}, \boldsymbol{u})t]\, \mathrm{d}\boldsymbol{r}. \tag{4}$$

On the other hand, as stated at the beginning of this paper, the projection of the density function is the spectrum of the signal $V_{\theta\varphi}(t)$,

$$P_{\theta\varphi}(\omega) = V_{\theta\varphi}(t) \exp(-\mathrm{i}\omega t)\, \mathrm{d}t.$$

When the phase-detected frequency ω is expressed in terms of the magnetic field β, $\omega = \gamma\beta$, it becomes

$$P_{\theta\varphi}(\beta) = \int V_{\theta\varphi}(t) \exp(-\mathrm{i}\gamma\beta t)\, \mathrm{d}t. \tag{5}$$

Putting equation (4) into equation (5), we obtain

$$P_{\theta\varphi}(\beta) = 1/\gamma \int F(\boldsymbol{r})\delta(b - \beta)\, \mathrm{d}\boldsymbol{r} \tag{6}$$

where $\delta(b)$ is the Dirac delta function. This equation indicates that the projection $P_{\theta\varphi}(\beta)$ is a surface integral of the density function along the magnetic field contour $b(\boldsymbol{r}, \boldsymbol{u}) = \beta$.

2.2. *Rectilinear reconstruction and its PSF in 3D imaging*

Under a uniform main magnetic field and linear field gradients,

$b = b_g = G\boldsymbol{r} \cdot \boldsymbol{u}$, the projection becomes

$$P_{\theta\varphi}(\beta) = (1/G\gamma) \int F(\boldsymbol{r})\delta(\boldsymbol{r} \cdot \boldsymbol{u} - \beta/G)\, \mathrm{d}\boldsymbol{r}$$

$$= (1/G\gamma) p_{\theta\varphi}(s)$$

where $s = \beta/G$ and $p_{\theta\varphi}(s)$ is an integral of $F(\boldsymbol{r})$ over the plane normal to $\boldsymbol{u}$ and at a distance s from the origin of $\boldsymbol{r}$. Suppose f is the 3D Fourier transform of the density function F. Along a radial line in the Fourier domain, the function $f(\rho, \theta, \varphi)$ is a 1D Fourier transform pair of the projection $p_{\theta\varphi}(s)$ (Lai 1981). We have

$$f(\rho, \theta, \varphi) = p_{\theta\varphi}(s) \exp(\mathrm{i}2\pi\rho s)\, \mathrm{d}s$$

$$= \gamma \int_{-m}^{m} P_{\theta\varphi}(\beta) \exp(\mathrm{i}2\pi\rho\beta/G)\, \mathrm{d}\beta \tag{7}$$

where m is the maximum magnitude of the space-dependent field within the imaging volume. Combine equations (6) and (7),

$$f(\rho, \theta, \varphi) = \int F(\boldsymbol{r}) \exp[\mathrm{i}2\pi\rho b(\boldsymbol{r}, \boldsymbol{u})/G]\, \mathrm{d}\boldsymbol{r}. \tag{8}$$

In the rectilinear filtered back projection, the density function is reconstructed by an inverse 3D Fourier transform on f (Lai 1981),

$$F_3(\boldsymbol{r}') = \int f(\rho, \theta, \varphi) \exp[-\mathrm{i}2\pi(\boldsymbol{\rho} \cdot \boldsymbol{r}')]\, \mathrm{d}\boldsymbol{\rho}. \tag{9}$$

Execution of this integral in spherical coordinates yields

$$F_3(\boldsymbol{r}') = \int_0^{2\pi} \mathrm{d}\varphi \int_0^{\pi} \sin\theta\, \mathrm{d}\theta \int_0^{M} \rho^2 f(\rho, \theta, \varphi) \times \exp[-\mathrm{i}2\pi\rho(\boldsymbol{r}' \cdot \boldsymbol{u})]\, \mathrm{d}\rho \tag{10}$$

where M is the cutoff frequency of the projections in the Fourier transform domain. Notice that

$$\boldsymbol{\rho} = \rho\boldsymbol{u} \tag{11}$$

as ρ is held at the gradient direction (θ, φ) in the partial integral with respect to ρ. The scalar product $\boldsymbol{r}' \cdot \boldsymbol{u}$ represents the projection of the vector $\boldsymbol{r}'$ along the gradient direction. According to equation (10), the 3D image $F(\boldsymbol{r}')$ is reconstructed by back projecting the 1D Fourier transform of $\rho^2 f$ for every gradient orientation.

To find the PSF, substitute equation (8) into equation (9)

$$F_3(\boldsymbol{r}') = \iint F(\boldsymbol{r}) \exp[\mathrm{i}2\pi(\rho b/G - \boldsymbol{\rho} \cdot \boldsymbol{r}')\, \mathrm{d}\boldsymbol{\rho}\, \mathrm{d}\boldsymbol{r}$$

$$= \int K_3(\boldsymbol{r}', \boldsymbol{r}) F(\boldsymbol{r})\, \mathrm{d}\boldsymbol{r} \tag{12}$$

where

$$K_3(\boldsymbol{r}', \boldsymbol{r}) = \int \exp[\mathrm{i}2\pi(\rho b/G - \boldsymbol{\rho} \cdot \boldsymbol{r}')]\, \mathrm{d}\boldsymbol{\rho}. \tag{13}$$

In equation (12) the convolution of the kernel K_3 with the density function $F(\boldsymbol{r})$ in the object coordinates results in the density function $F_3(\boldsymbol{r}')$ in the image coordinates. Obviously, the real part of K_3 is the PSF of the image under reconstruction. Applying equations (2), (3) and (11), the 3D PSF becomes

$$K_3(\boldsymbol{r}', \boldsymbol{r}) = \int \exp[\mathrm{i}2\pi(\rho\boldsymbol{r} \cdot \boldsymbol{u} + \rho b_0/G - \boldsymbol{\rho} \cdot \boldsymbol{r}')]\, \mathrm{d}\boldsymbol{\rho}$$

$$= \int \exp[\mathrm{i}2\pi(\boldsymbol{r} \cdot \boldsymbol{\rho} - \boldsymbol{\rho} \cdot \boldsymbol{r}' + \rho b_0/G)]\, \mathrm{d}\boldsymbol{\rho}$$

Let

$$\boldsymbol{R} = \boldsymbol{r} - \boldsymbol{r}' \tag{14}$$

we have

$$K_3(\boldsymbol{r}', \boldsymbol{r}) = \int \exp[\mathrm{i}2\pi\rho b_0(\boldsymbol{r})/G] \exp[\mathrm{i}2\pi\boldsymbol{\rho} \cdot \boldsymbol{R}]\, \mathrm{d}\boldsymbol{\rho}. \tag{15}$$

Equation (15) shows that K_3 is a 3D Fourier transform of the function $\exp(\mathrm{i}2\pi\rho b_0/G)$. Since the function depends only on the radial coordinate ρ, the 3D Fourier transform can be simplified to (Champeney 1972)

$$K_3(\boldsymbol{r}', \boldsymbol{r}) = \int_0^{M} \exp(\mathrm{i}2\pi\rho b_0/G) \frac{\sin(2\pi\rho R)}{2\pi\rho R} 4\pi\rho^2\, \mathrm{d}\rho. \tag{16}$$

When the main magnetic field is uniform, $b_0(\boldsymbol{r}) = 0$, the PSF reduces to

$$\mathrm{Re}\, K_3(\boldsymbol{r}', \boldsymbol{r}) = \frac{3}{4\pi M^3} \int_0^{M} \frac{\sin(2\pi\rho R)}{2\pi\rho R} 4\pi\rho^2\, \mathrm{d}\rho$$

$$= \frac{3}{(2\pi MR)^2}\left(\frac{\sin(2\pi MR)}{2\pi MR} - \cos(2\pi MR)\right) \tag{17}$$

where a normalisation factor of $3/4\pi M^3$ is used. This 3D PSF has spherical symmetry since it depends only on R. It is plotted against the radial distance R in curve A of figure 1, where R is in the units of $1/M$. It should be noted that following a discrete Fourier transform in equation (10) the interval between adjacent data points is $1/M$. Assuming this interval is equal to that

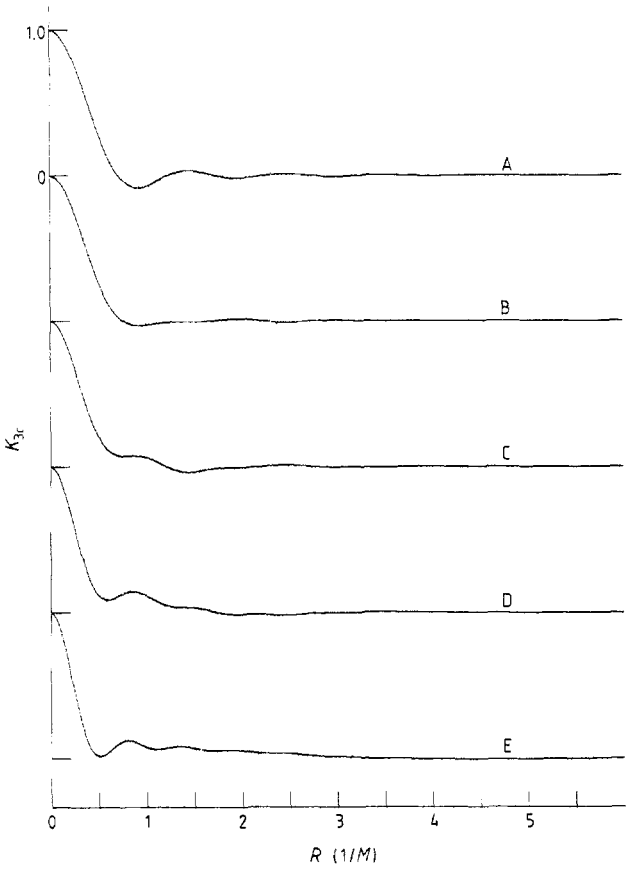

Figure 1. A, The near-region PSF of 3D reconstruction versus the radial distance in a uniform main magnetic field. B–E, the PSF of 3D curvilinear reconstruction under inhomogeneous main magnetic field at the differential inhomogeneity of $\Delta b/G = 0.2R$, $0.4R$, $0.6R$ and $0.8R$ respectively. The vertical scales are identical, but only the top one is labelled.

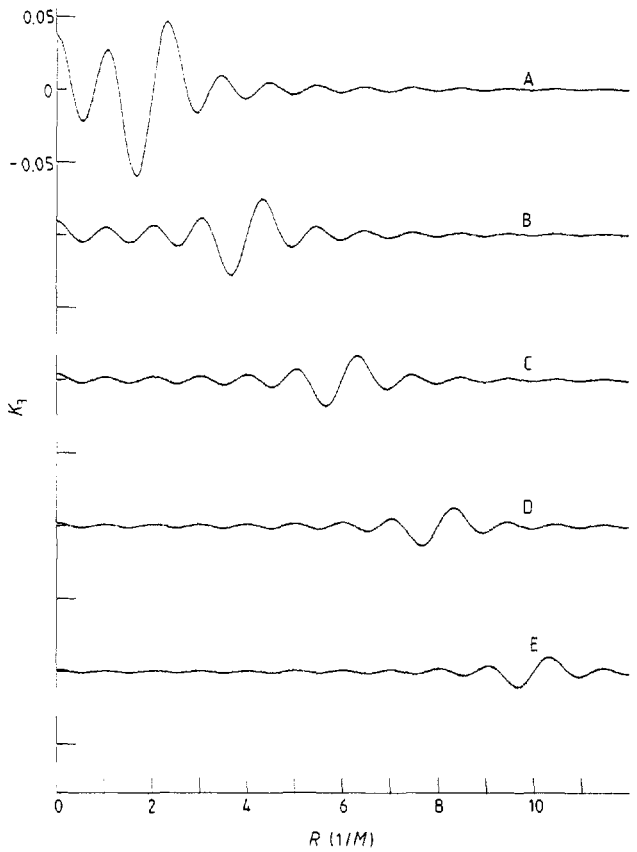

Figure 2. Plots of the PSF in 3D rectilinear reconstruction at the local inhomogeneities b_0/G of A, 2; B, 4; C, 6; D, 8 and E, 10 units. Like the previous one and the following two figures, the vertical scales are unified and labelled in A.

between adjacent picture elements (pixels), as it usually is, we can regard the coordinate in figure 1 as being in pixel units.

When the field is inhomogeneous, $b_0(\boldsymbol{r}) \neq 0$, the 3D PSF is space dependent,

$$\begin{aligned}\mathrm{Re}\, K_3(\boldsymbol{r}', \boldsymbol{r}) &= \frac{3}{4\pi M^3}\frac{2}{R}\int_0^M \cos[2\pi\rho b_0(\boldsymbol{r})/G]\sin(2\pi\rho R)\rho\, \mathrm{d}\rho \\ &= \frac{3}{8\pi^2 M^2 R(R+b_0/G)}\left(\frac{\sin 2\pi M(R+b_0/G)}{2\pi M(R+b_0/G)}\right. \\ &\quad \left. - \cos 2\pi M(R+b_0/G)\right) + \frac{3}{8\pi^2 M^2 R(R-b_0/G)} \\ &\quad \times \left(\frac{\sin 2\pi M(R-b_0/G)}{2\pi M(R-b_0/G)}\right. \\ &\quad \left. - \cos 2\pi M(R-b_0/G)\right). \end{aligned} \tag{18}$$

As in the case of uniform field, the PSF in the far region, $R \gg b_0/G$, is negligibly small compared to that in the near region. In the near region, the local field can be approximated by a constant since the magnetic field normally does not vary appreciably over a small region. The PSF's at local inhomogeneities of $b_0/G = 2$, 4, 6, 8 and 10 in units of $1/M$, i.e. pixel units, are plotted in figure 2. The peak no longer occurs at $R = 0$ but is displaced toward $R \cong b_0/G$. The amplitude of the peak also decreases considerably as b_0 increases. However, this PSF is a 3D function, and the peak describes a spherical shell in the 3D representation. The total PSF per unit thickness of this shell actually increases slightly as b_0 increases. Since the radius of the shell enlarges as the inhomogeneity increases, the reconstructed image would be blurred. To improve the image resolution, the only deblurring technique available so far is the application of strong field gradients, which reduce the magnitude of b_0/G in equation (18).

2.3. *Curvilinear reconstruction and its PSF in 3D imaging*

The inhomogeneity $b_0(\boldsymbol{r})$ in equation (18) represents the deviation of the local field from a reference known as the projection centre for the reconstruction. If b_0 were replaced by a differential inhomogeneity, Δb, measured with respect to the local point to be reconstructed, namely $b_0(\boldsymbol{r}) - b_0(\boldsymbol{r}')$, the width of the PSF would be greatly narrowed since the differential inhomogeneity is small within the near region and vanishes at $R = 0$. An additional term, $\exp[-\mathrm{i}2\pi\rho b_0(\boldsymbol{r}')/G]$, would be needed in the integral of equation (15), which derived from equation (9). Thus, in order to obtain sharp images, we modify the reconstruction (9) to

$$\begin{aligned} F_{3c}(\boldsymbol{r}') &= \int \exp[-\mathrm{i}2\pi\rho b_0(\boldsymbol{r}')/G] f(\rho, \theta, \varphi) \exp[-\mathrm{i}2\pi(\boldsymbol{\rho}\cdot\boldsymbol{r}')]\, \mathrm{d}\rho \\ &= \int_0^{2\pi} \mathrm{d}\varphi \int_0^{\pi} \sin\theta\, \mathrm{d}\theta \int_0^M \rho^2 f \\ &\quad \times \exp\{-\mathrm{i}2\pi\rho[\boldsymbol{r}'\cdot\boldsymbol{u} + b_0(\boldsymbol{r}')/G]\}\, \mathrm{d}\rho. \end{aligned} \tag{19}$$

Since the equation $\boldsymbol{r}' \cdot \boldsymbol{u} = \text{const}$ is a plane in the 3D image space, $\boldsymbol{r}' \cdot \boldsymbol{u} + b_0(\boldsymbol{r}')/G = \text{const}$ represents a curved surface deviating from the plane by $b_0(\boldsymbol{r}')/G$. Equation (19) is, in fact, a curvilinear filtered back projection of the 1D Fourier transform result onto a family of surfaces.

Following the derivation in the section above, the inhomogeneity-corrected 3D kernel becomes

$$K_{3c}(\boldsymbol{r}', \boldsymbol{r}) = \int \exp\{\mathrm{i}2\pi\rho[b_0(\boldsymbol{r}) - b_0(\boldsymbol{r}')]/G\} \exp(\mathrm{i}2\pi\boldsymbol{\rho} \cdot \boldsymbol{R})\, \mathrm{d}\boldsymbol{\rho}.$$

Denote

$$\Delta b(\boldsymbol{r}', \boldsymbol{r}) = b_0(\boldsymbol{r}) - b_0(\boldsymbol{r}'). \tag{20}$$

The corrected 3D PSF has

$$\begin{aligned}\mathrm{Re}\, K_{3c}(\boldsymbol{r}', \boldsymbol{r}) = {} & \frac{3}{8\pi^2 M^2 R(R + \Delta b/G)} \left(\frac{\sin 2\pi M(R + \Delta b/G)}{2\pi M(R + \Delta b/G)} \right. \\ & \left. - \cos 2\pi M(R + \Delta b/G) \right) + \frac{3}{8\pi^2 M^2 R(R - \Delta b/G)} \\ & \times \left(\frac{\sin 2\pi M(R - \Delta b/G)}{2\pi M(R - \Delta b/G)} - \cos 2\pi M(R - \Delta b/G) \right). \end{aligned} \tag{21}$$

Comparison of equations (21) and (17) indicates that the corrected PSF at R is about the average of the uniform field PSF at $R - \Delta b/G$ and $R + \Delta b/G$. Within a small local region, the differential inhomogeneity is small and linear in the first order approximation,

$$\Delta b/G \cong \alpha R \qquad \text{with} \qquad 0 \leqslant \alpha \leqslant 1.$$

The parameter α represents the gradient of the field inhomogeneity. For instance, at $\alpha = 0.4$ it is equivalent to 40% of the gradient strength generated by the gradient coils. The corrected 3D PSF's of $\alpha = 0.2$, 0.4, 0.6 and 0.8 are delineated in curves B–E of figure 1.

It is the gradient of the inhomogeneity, rather than the inhomogeneity itself, which determines the shape of this PSF. All the PSF's shown in curves B–E peak at the centre and are, in general, well behaved. The PSF at $\alpha = 0.2$ even appears better than the uniform field case in curve A. As R increases toward the far region, the PSF's converge to zero rapidly, regardless of the magnitude of α. This technique should allow us to reconstruct 3D images of high fidelity.

2.4. Reconstruction technique and PSF in 2D imaging

Two-dimensional tomography reconstruction is a special case of the 3D volume reconstruction described above, with the polar coordinate θ fixed at $\pi/2$. The gradient unit vector $\boldsymbol{u}$, the object coordinate $\boldsymbol{r}$ and the image coordinate $\boldsymbol{r}'$ are all limited to the xy plane. The density function in the object space, $F(\boldsymbol{r})$, in the image space, $F(\boldsymbol{r}')$, and in the Fourier domain, $f(\rho, \varphi)$, are 2D functions. From equation (9), the rectilinear reconstruction for 2D imaging

$$\begin{aligned} F_2(\boldsymbol{r}') &= \int f(\rho, \varphi) \exp[-\mathrm{i}2\pi(\boldsymbol{\rho} \cdot \boldsymbol{r}')]\, \mathrm{d}\boldsymbol{\rho} \\ &= \int_0^{2\pi} \mathrm{d}\varphi \int_0^M \rho f(\rho, \varphi) \exp[-\mathrm{i}2\pi(\boldsymbol{r}' \cdot \boldsymbol{u})\, \mathrm{d}\rho \end{aligned} \tag{22}$$

has 2D kernel

$$K_2(\boldsymbol{r}', \boldsymbol{r}) = \int \exp[\mathrm{i}2\pi\rho b_0(\boldsymbol{r})/G] \exp(\mathrm{i}2\pi\boldsymbol{\rho} \cdot \boldsymbol{R})\, \mathrm{d}\boldsymbol{\rho}$$

and the 2D PSF

$$\mathrm{Re}\, K_2(\boldsymbol{r}', \boldsymbol{r}) = \int \cos[2\pi\rho b_0(\boldsymbol{r})/G] \exp(\mathrm{i}2\pi\boldsymbol{\rho} \cdot \boldsymbol{R})\, \mathrm{d}\boldsymbol{\rho}.$$

This integral, a 2D Fourier transform of a function which depends only on the modulus of $\boldsymbol{\rho}$, can be reduced to 1D integration of a Bessel function (Champeney 1972),

$$\mathrm{Re}\, K_2(\boldsymbol{r}', \boldsymbol{r}) = 2\pi \int_0^M \rho \cos[2\pi\rho b_0(\boldsymbol{r})/G] J_0(2\pi\rho R)\, \mathrm{d}\rho. \tag{23}$$

Based on properties of Bessel functions, the integral can be carried out for $b_0 = 0$. After normalisation we have

$$\mathrm{Re}\, K_2(\boldsymbol{r}', \boldsymbol{r}) = (1/\pi MR) J_1(2\pi MR).$$

This 2D PSF in uniform magnetic field is shown in curve A of figure 3.

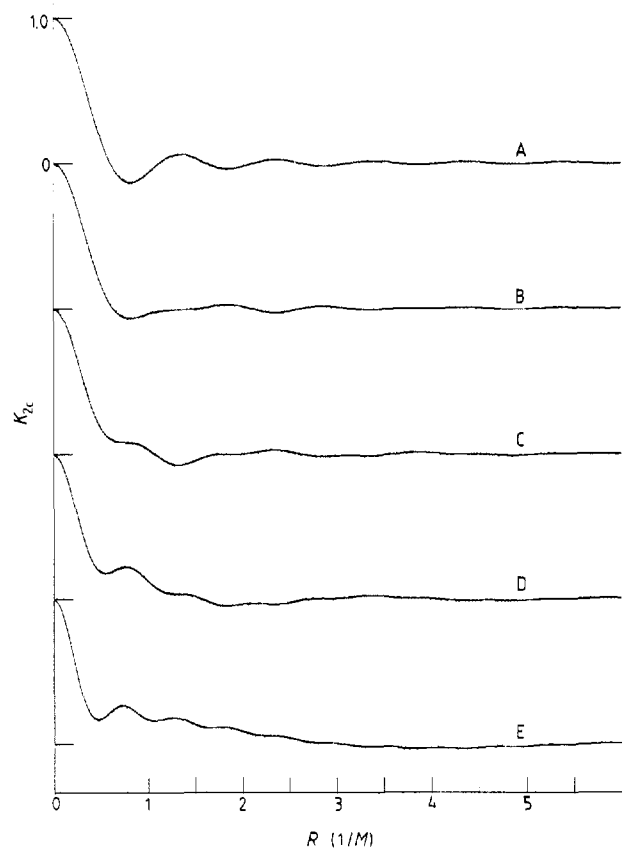

Figure 3. A, The PSF of 2D reconstruction in a uniform magnetic field. B–E, The PSF of 2D curvilinear reconstruction at differential inhomogeneity of $\Delta b/G = 0.2R$, $0.4R$, $0.6R$ and $0.8R$ respectively.

For $b_0 \neq 0$, the integral in equation (23) cannot be expressed in a closed form. Numerical methods are used to plot the PSF for $b_0/G = 2$, 4, 6, 8 and 10 units in figure 4. In 2D representation, the peak of the PSF describes a circular ring. The outward spread of the PSF will rapidly blur the image as the inhomogeneity increases.

Like equation (19), the inhomogeneity-corrected 2D reconstruction can be written as

$$F_{2c}(\boldsymbol{r}') = \int_0^{2\pi} \mathrm{d}\varphi \int_0^M \rho f \exp\{\mathrm{i}2\pi\rho[\boldsymbol{r}' \cdot \boldsymbol{u} + b_0(\boldsymbol{r}')/G]\}\, \mathrm{d}\rho. \tag{24}$$

Here it is a curvilinear back projection of the Fourier transform onto a family of curves. Using the differential inhomogeneity in equation (20) and following the derivation for equation (23), we

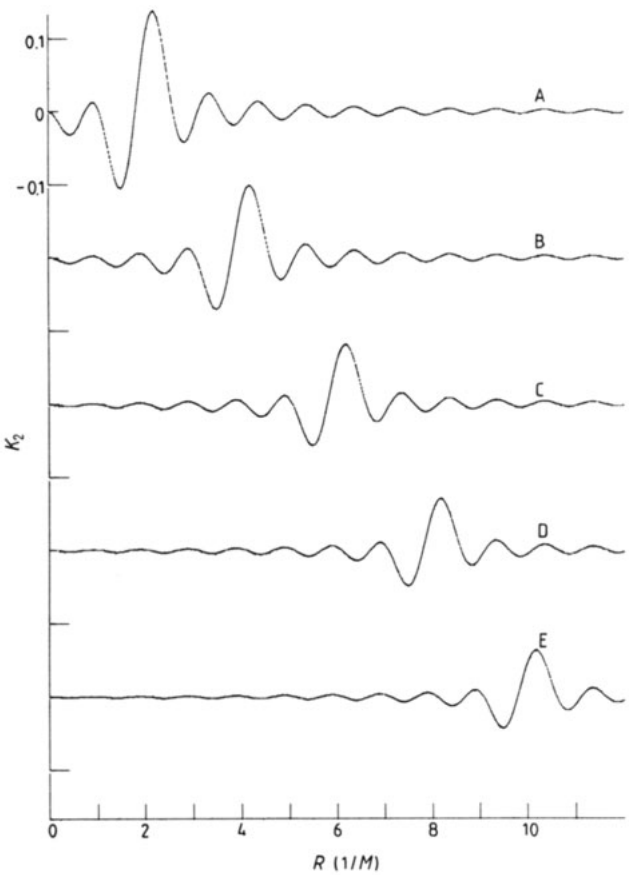

Figure 4. The near-region PSF in 2D rectilinear reconstruction at the local inhomogeneity $b_0(G$ of 2, 4, 6, 8 and 10 units, respectively, for A–E.

obtain the normalised PSF

$$\mathrm{Re}\, K_{2c}(\boldsymbol{r}', \boldsymbol{r}) = \frac{2}{M^2} \int_0^M \rho \cos(2\pi\rho\Delta b/G) J_0(2\pi\rho R)\, \mathrm{d}\rho. \quad (25)$$

In the local region, the inhomogeneity-corrected 2D PSF's for $\Delta b/G = 0.2R$, $0.4R$, $0.6R$ and $0.8R$ are plotted in curves B–E of figure 3. These narrow PSF's keep the 2D images from blurring.

3. Experiments by computer simulations

An object consisting of five circular discs is constructed on a 128×128 matrix. The discs have uniform and identical densities. The largest, with a radius of 14 pixels, is located at the centre. The others, with radii of 10, 9, 8 and 7 pixels, are each near one of the four corners of the matrix. Based on a field distribution, 180 projections of the object are computed according to equation (6). Each projection is digitised into 128 data points. The projections are then filtered and back projected onto the image space of 128×128 pixels. In the first experiment, the field is homogeneous. The reconstructed image is shown in figure 5, with the intensity displayed as a 2D function against the pixel coordinates. The reconstruction noises, intensified by the sharp edges of the object, are visible.

An inhomogeneous field of

$$b_0(x', y')/G = 10[(x'-60)^2 + (y'-60)^2]/4096$$

is arbitrarily selected for the next experiment. The inhomogeneity is expressed in pixel units, with one pixel unit equivalent to the field difference resulting from the applied field gradient over one-pixel distance. In this scale, $b_0(x', y')/G$ represents the

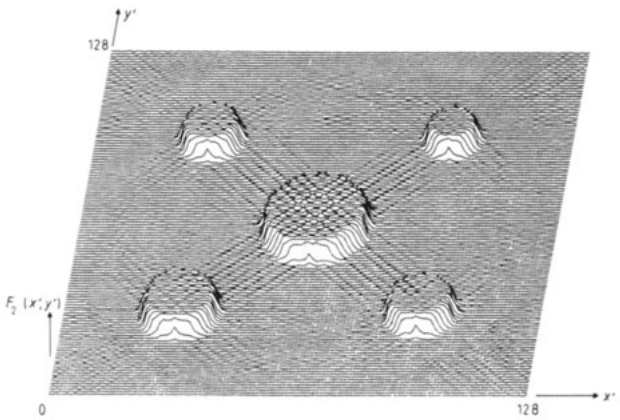

Figure 5. Result of 2D imaging simulation on a five-disc phantom placed in a uniform main magnetic field. Image intensities are displayed by the amplitudes in 128 curves, each associated with 128 data points, representing the 128×128 pixels.

number of pixels by which the point at (x', y') has departed from the straight projection path in the uniform field, into the curved path on which it now lies. This field distribution in $x'y'$ plane is depicted in figure 6. At the corners the inhomogeneity reaches about 10 pixel units. The field is at least an order of magnitude less uniform than in the first experiment, where inhomogeneities of less than one pixel unit are assumed. The image reconstructed by the conventional, rectilinear, filtered back projection is much blurred and distorted, as is shown in figure 7. But the curvilinear reconstruction technique, described in equations (24) and (30), produces a sharp and accurate picture as displayed in figure 8.

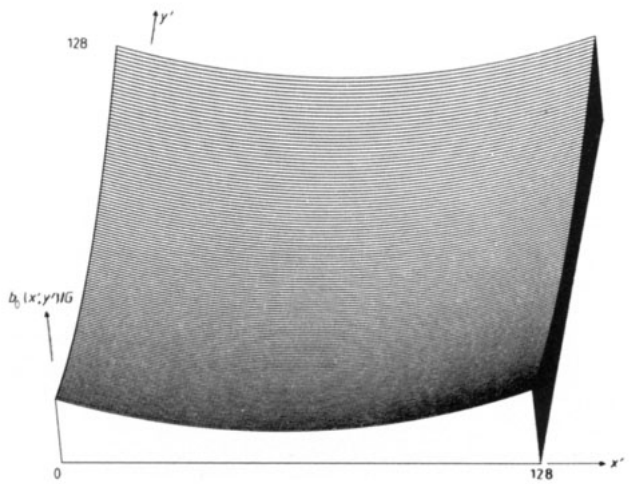

Figure 6. The field distribution of the quadratic inhomogeneity $b_0(x', y')$ plotted against the pixel coordinates in pixel units. The minimum field in this $x'y'$ plane occurs at the pixel (60, 60).

Also, reconstruction noises are reduced. This may result from the variations in width and orientation of the curvilinear paths, which make the back projection pattern less symmetrical and, therefore, make reconstruction noise accumulations at a given pixel less coherent.

The orientations of these 180 projections are one degree apart, but the gradient directions are reversed for every other

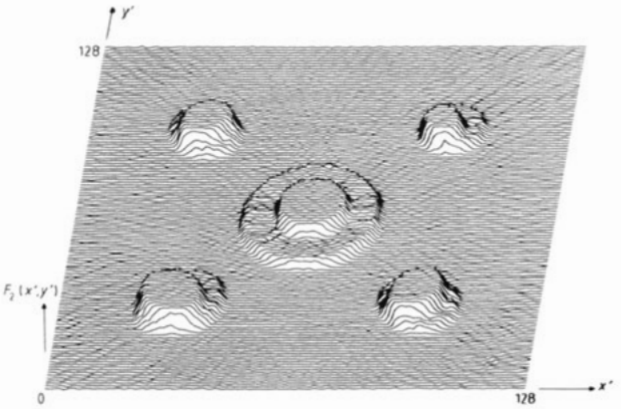

Figure 7. Image of the phantom in the inhomogeneous field by the conventional rectilinear reconstruction.

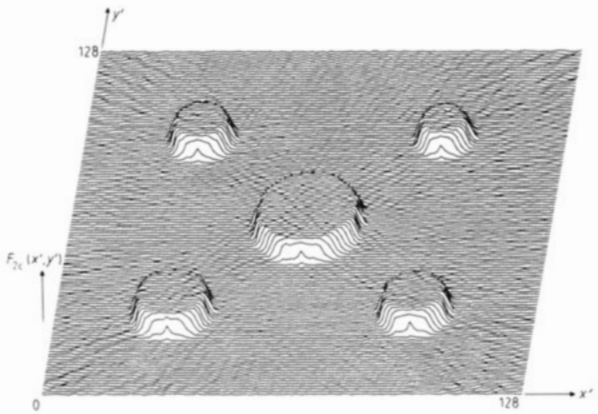

Figure 8. Image reconstructed by the new curvilinear technique of the phantom in the inhomogeneous field. Like figures 5 and 7, it is reconstructed from 180 projections with the projection orientations extended over 360°.

projection, so that the projections actually extend over 360°. In the case of a homogeneous field, it makes no difference whether the projection angles cover 180° or 360°. Contrariwise, the range of the projection angles does affect the accuracy of an image taken from inhomogeneous fields. For comparison with figure 8, a curvilinear reconstruction of the object from projections oriented within 180° range is given in figure 9. The picture seems to retain its sharpness, but sizable artefacts arise. Intensity variations among the five discs are also evident.

4. Other considerations

Comparison of equations (4) and (8) shows that

$$f(\rho, \varphi) = V_\varphi(\rho/\gamma G)$$

in 2D notation. Equation (24) could be written as

$$F_{2c}(\boldsymbol{r}') = (\gamma G)^2 \int_0^{2\pi} \mathrm{d}\varphi \int_0^{M/\gamma G} t V_\varphi(t) \times \exp\{-\mathrm{i}2\pi\gamma G t[(\boldsymbol{r}' \cdot \boldsymbol{u}) + b_0(\boldsymbol{r}')/G]\}\, \mathrm{d}t. \qquad (26)$$

Indeed, the availability of time-domain NMR signals allows simpler computation for the reconstruction. The back projection could be performed directly from the Fourier transform of the NMR signal multiplied by t in 2D imaging, or t^2 in 3D imaging (Lai 1981).

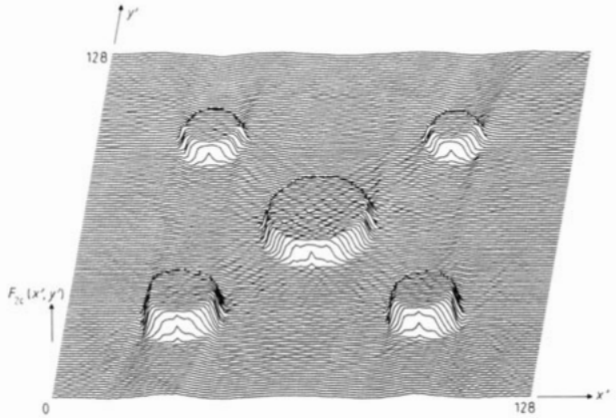

Figure 9. Curvilinear reconstruction of the image with the same number of projections but confining the orientations within 180° range.

Usually the NMR signal $V(t)$ exists only for $t \geqslant 0$, $F(\boldsymbol{r}')$ is in general a complex function unless special echo techniques are used to generate a symmetrical $V(t)$ function. The real part of $F(\boldsymbol{r}')$ is the image reconstructed from the absorption-mode NMR signal, while the imaginary part of $F(\boldsymbol{r}')$ comes from the dispersion mode. Since the dispersion-mode spectrum does not represent a true projection, the imaginary part of $F(\boldsymbol{r}')$ does not resemble the object $F(\boldsymbol{r})$. It is normally discarded.

In the special case of uniform magnetic fields, as the gradient reverses its direction we have

$$b(\boldsymbol{r}, -\boldsymbol{u}) = b_g(\boldsymbol{r}, -\boldsymbol{u}) = -b(\boldsymbol{r}, \boldsymbol{u}). \qquad (27)$$

Since $F(\boldsymbol{r})$ is real and $\boldsymbol{u}(\varphi + \pi) = -\boldsymbol{u}(\varphi)$ in 2D coordinates, equations (4) and (27) lead to

$$V_{\varphi+\pi}(t) = V_\varphi^*(t).$$

Consequently, for $b_0 = 0$ we can partition the φ integration of equation (26) into two halves and recombine them,

$$\begin{aligned} \mathrm{Re}\, F_2(\boldsymbol{r}') &= (\gamma G)^2\, \mathrm{Re} \int_0^{\pi} \mathrm{d}\varphi \int_0^{M/\gamma G} t\{V_\varphi \exp[-\mathrm{i}2\pi\gamma G t(\boldsymbol{r}' \cdot \boldsymbol{u})] \\ &\quad + V_\varphi^* \exp[\mathrm{i}2\pi\gamma G t(\boldsymbol{r}' \cdot \boldsymbol{u})]\}\, \mathrm{d}t \\ &= 2(\gamma G)^2\, \mathrm{Re} \int_0^{\pi} \mathrm{d}\varphi \int_0^{M/\gamma G} t V_\varphi \\ &\quad \times \exp[-\mathrm{i}2\pi\gamma G t(\boldsymbol{r}' \cdot \boldsymbol{u})]\, \mathrm{d}t. \end{aligned} \qquad (28)$$

It is sufficient to steer the gradient vector over an angle of π for reconstructing $F_2(\boldsymbol{r}')$.

However, when the field is inhomogeneous it is obvious that

$$V_{\varphi+\pi}(t) \neq V_\varphi^*(t).$$

The integrand in equation (26) at one gradient direction is in general not a complex conjugate of the opposite one. It requires full range of 2π in φ to reconstruct $F_{2c}(\boldsymbol{r}')$, or 4π solid angle in (θ, φ) for reconstructing the 3D image $F_{3c}(\boldsymbol{r}')$.

Another way of looking at this matter is to consider the local field as uniform but with an intrinsic and stationary field gradient ∇b_0. As the external field gradient is steered from $\varphi = 0$ to π, the total gradient ∇b does not rotate exactly π radian, as illustrated in figure 10. Some of the projection views in the local region will be either redundant or missing. The reconstruction is not quite accurate, as shown in figure 9.

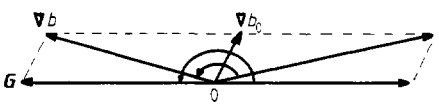

Figure 10. The role of nonvanishing intrinsic gradient ∇b_0 at a local point. Although the applied field gradient $\boldsymbol{G}$ rotates through 180°, the resultant field gradient ∇b does not cover 180° nor does it have a constant strength.

It should be noted that

$$f(\rho, \varphi) = \gamma \int_{-m}^{m} P_\varphi(\beta) \exp[\mathrm{i}2\pi\rho\beta/G)\, \mathrm{d}\beta$$

is ranged from $\rho = -M$ to $+M$. If the image were actually calculated from $f(\rho, \varphi)$, which is obtained from P_φ in the equation above, we should write

$$F_{2c}(\boldsymbol{r}') = 1/2 \int_0^{2\pi} \mathrm{d}\varphi \int_{-M}^{M} |\rho| f(\rho, \varphi) \times \exp\{-\mathrm{i}2\pi\rho[\boldsymbol{r}' \cdot \boldsymbol{u} + b_0(\boldsymbol{r}')/G]\}\, \mathrm{d}\rho.$$

Again, when the field is uniform

$$f(\rho, \varphi + \pi) = f(-\rho, \varphi). \tag{29}$$

Using the fact that the Fourier transforms of both $|\rho|$ and f are real, it can be shown that

$$F_2(\boldsymbol{r}') = \int_0^{\pi} \mathrm{d}\varphi \int_{-M}^{M} |\rho| f(\rho, \varphi) \exp[-\mathrm{i}2\pi\rho(\boldsymbol{r}' \cdot \boldsymbol{u})]\, \mathrm{d}\rho.$$

However, under inhomogeneous field equation (29) is not valid and the full range of φ must be used for the integral.

In numerical calculation, integrals are replaced by summations. Consequently, each data point of a projection is a summation of $F(\boldsymbol{r})$ along a curved strip of finite but variable width. If the reconstruction were executed by back projecting the Fourier-transformed result one point at a time onto this strip, the calculation would be tedious since we would have to find all pixels lying within this strip. These pixels are defined by

$$L - 1/2 \leqslant \boldsymbol{r}' \cdot \boldsymbol{u} + b_0(\boldsymbol{r}')/G \leqslant L + 1/2$$

where L, in the unit $1/M$, is the centre of strip L. From the practical point of view, it is better to perform the reconstruction by sequentially scanning through the pixels and to find the strip which runs through them from the equation

$$L = \boldsymbol{r}' \cdot \boldsymbol{u} + b_0(\boldsymbol{r}')/G. \tag{30}$$

The Fourier-transformed datum at L is then added to the pixel at $\boldsymbol{r}'$, as indicated in equation (19) or (24). Since the pixel has finite size, it may not fall completely into one path. The value to be added to $\boldsymbol{r}'$ is normally interpolated between two adjacent data points.

At the expense of computation time, it may be possible to calculate NMR images by an iterative reconstruction algorithm. The iterative technique requires back projections as well as forward projections. The pixel scanning procedure described is applicable to both operations, except that in forward projection the pixel value is added to the Lth data point instead.

The magnetic field is not necessarily operated at on-resonance condition, especially in the single-phase detection system where the field is often offset by a considerable amount. The field offset is embedded in $b_0(\boldsymbol{r})$ as a constant. Equation (30) indicates that every Fourier-transformed result must be shifted by this offset constant, i.e., there must be a proper centring of the projection profile (Lai and Lauterbur 1981), before back projecting it to the pixels. The PSF is not affected by the field offset, since the offset is cancelled by both terms in equation (20). However, if the shift were inaccurate, $\Delta b \neq 0$ even at $R = 0$, the image would be blurred.

5. Conclusions

Image blurring due to an inhomogeneous magnetic field can be avoided by a curvilinear back projection technique. Computer simulations clearly show that the main magnetic field for projection-reconstruction of NMR images need not possess the high degree of homogeneity that has been supposed. However, the field gradient $\boldsymbol{G}$ must be steered through a full angular range of 2π in 2D imaging, and 4π solid angle in 3D imaging.

Commercially available magnets, aided by shim coils, are currently specified at about 15 PPM inhomogeneity over a working volume of approximately 400 mm diameter for medical imagings. The inhomogeneity in the experiment described above is already an order of magnitude larger. The actual limit of inhomogeneity that this technique can successfully deal with remains to be investigated. Undoubtedly, it should be able to correct for the inherent inhomogeneities of commercial magnets as well as for the field distortion caused by surrounding materials. This technique's allowance for non-uniformities in the magnetic field should also make it easier to achieve high-resolution imaging than is possible in rectilinear reconstructions. In addition, since the projection paths need not be straight, the field gradient strength can be reduced. Consequently, not only the NMR signal quality is enhanced, but also the construction for linear gradient coils can be eased.

The PSF is a function of the differential inhomogeneity Δb and the radial distance R measured with respect to the point of interest. As long as the gradient of the inhomogeneity ∇b_0 is small compared to the strength of the applied gradient G, the PSF remains narrow and well behaved everywhere. Therefore, when the field varies gradually and continuously over the regions, the field difference between two distant points can be substantial and still yield high-fidelity images. However, inhomogeneities which change rapidly in local areas, having large ∇b_0, are less acceptable, although the overall inhomogeneity might be smaller.

The magnetic susceptibility of the object can slightly disturb the field, especially when the magnet is operated at high field or when the object is a nonbiological sample of high susceptibility. If the field distribution can be measured with the object in place, the curvilinear reconstruction technique can still be applied to correct for the perturbation introduced by the object itself. It is worth noting that a modified NMR imaging technique for rapidly measuring magnetic field distribution within the object has been proposed and demonstrated (Maudsley *et al* 1979).

In summary, the curvilinear reconstruction technique presented here is a promising way of obtaining accurate NMR images under inhomogeneous magnetic field. With this technique, the uniformity requirement of the magnet, whether resistive or superconductive, becomes far less stringent. The technique not only can reduce the cost of an NMR imaging system, but also make the system more durable and practical for clinical use. Furthermore, given the same degree of field uniformity, more accurate and higher resolution images can be reconstructed by this technique than by the conventional rectilinear technique.

References

Champeney D C 1972 *Fourier Transforms and their Physical Applications* (New York: Academic Press)

Hinshaw W S 1976 Image formation by nuclear magnetic resonance: the sensitive point method
J. Appl. Phys. **47** 3709–21

Hutchison J M S, Sutherland R J and Mallard J R 1978 NMR imaging: image recovery under magnetic fields with large non-uniformities
J. Phys. E: Sci. Instrum. **11** 217–21

Lai C-M and Lauterbur P C 1980 A gradient control device for complete three-dimensional nuclear magnetic resonance zeugmatographic imaging
J. Phys. E: Sci. Instrum. **13** 747–50

Lai C-M and Lauterbur P C 1981 Automatic correction of nuclear magnetic resonance zeugmatographic projections
J. Phys. E: Sci. Instrum. **14** 874–9

Lai C-M 1981 True three-dimensional nuclear magnetic resonance imaging by Fourier reconstruction zeugmatography
J. Appl. Phys. **52** 1141–5

Maudsley A A, Oppelt A and Ganssen A 1979 Rapid measurement of magnetic field distributions using nuclear magnetic resonance
Siemens R/D Report vol **8**, 6 326–31